

## Functional Characterization of the Amino-Terminal Region of Myosin-2

Setsuko Fujita-Becker<sup>‡</sup>, Georgios Tsiavaliaris<sup>§</sup>, Reiko Ohkura<sup>¶</sup>, Takashi Shimada<sup>¶</sup>, Dietmar J. Manstein<sup>\*,§</sup>, and Kazuo Sutoh<sup>¶</sup>

From the <sup>‡</sup>Max-Planck-Institut für Medizinische Forschung, Jahnstr. 29, 69120 Heidelberg, Germany;

<sup>§</sup>Medizinische Hochschule Hannover, Institut für Biophysikalische Chemie, Carl-Neubergstr.1, 30623 Hannover, Germany, <sup>¶</sup>Department of Life Science, University of Tokyo, Komaba 3-8-1, Tokyo 153-8902, Japan.

Running Title: N-terminal region of myosin-2

Address correspondence to Dietmar J. Manstein, MHH, Institute for Biophysical Chemistry, OE4350, 30625 Hannover, Germany. T: +49-511-5323700; F: +49-511-532-5966; E-mail: manstein@bpc.mh-hannover.de

All class-2 myosins contain an amino-terminal extension of approximately 80 residues that includes an SH3-like subdomain. To explore the functional importance of this region, which is also present in most other myosin classes, we generated truncated constructs of *Dictyostelium discoideum* myosin-2. Truncation at position 80 resulted in the complete loss of myosin-2 function *in vivo*. Actin affinity was more than 80-fold and the rate of ADP release approximately 40-fold decreased in this mutant. In contrast, a myosin construct that lacks only the SH3-like subdomain, corresponding to residues 33-79, displayed much smaller functional defects. In complementation experiments with myosin-2 null cells, this construct rescued myosin-2-dependent processes such as cytokinesis, fruiting body formation and sporogenesis. An 8-fold reduction in motile activity and changes of similar extend in the affinity for ADP and filamentous actin indicate the importance of the SH3-like subdomain for correct communication between the functional regions within the myosin motor domain and suggest that local perturbations in this region can play a role in modulating myosin-2 motor activity.

Members of the myosin superfamily of actin-based motors act in a variety of cellular functions such as muscle contraction, cell and organelle movement, membrane trafficking, and signal transduction. Although myosin motor domains show a high degree of sequence conservation, the individual myosin classes are clearly defined by differences in the head structure (1). Extensive biochemical investigations of the myosin ATPase cycle together with structural information of the motor domain and electron microscopy of the actomyosin complex have led to detailed molecular models of the nucleotide-dependent actomyosin interaction (2,3). However, the exact functional roles of several regions of the myosin motor domain remain to be elucidated. In particular, the role of a protruding, six-stranded, antiparallel,  $\beta$ -barrel subdomain with similarities to SH3-domains, which appears to be present in most myosins and comprises approximately 50 amino acids of the heavy chain, is

largely unknown. The structure of this subdomain has been solved for class-2, -5 and -6 myosins (4-7). The crystal structure of the nucleotide-free smooth muscle myosin motor domain with essential light chain (ELC)<sup>1</sup> bound, shows the ELC to be in contact with the N-terminal domain of the heavy chain, but in the presence of MgADP•AlF<sub>4</sub><sup>-</sup> the ELC is rotated up to 70° from the position in nucleotide-free S1 and forms a contact with loop-1 (8).

Sequence alignments of the N-terminal region of myosins from different classes reveal that this region varies greatly in length and amino acid composition between the individual members. Class-1 myosins completely lack the N-terminal region corresponding to the first 79 residues of myosin-2 (9). In the case of class-2 myosins, residues 1-33 form an extended structure crossing the interface between motor domain and neck region (Figure 1). Residues from this segment are in close contact and cover a hydrophobic groove on the motor domain surface. The ensuing residues 33-79 form the SH3-like subdomain (10). Biochemical studies with zero-length cross linkers indicate that the two heads of myosin, when bound in a rigor complex with F-actin, are in close contact with each other. In the case of chicken gizzard HMM, Glu-168 could be cross-linked to Lys-65 in the SH3-like subdomain of the neighboring head (11). The cross-linked acto-HMM displayed a significantly increased ATPase activity, which was interpreted as evidence that this interaction may play a pivotal role in myosin function (12,13).

Here, we focus on the biological and biochemical properties of the N-terminal region of myosin-2. We use deletion mutants to elucidate the role of this region by analyzing the mutants' kinetic behavior and their ability to produce force and movement in an *in vitro* assay system. Complementation of *Dictyostelium discoideum* myosin-2 null cells is used for the *in vivo* analysis of the N-terminally truncated constructs. The characterization of the truncated myosins demonstrates that the removal of the SH3-like domain affects the interaction with nucleotides and actin as well as communication within the motor domain. Complete removal of the 80 amino acid long N-terminal region results in almost complete

loss of function and greatly aberrant kinetic properties.

## EXPERIMENTAL PROCEDURES

**Plasmid construction and transformation** – Standard chemicals were purchased from Sigma, restriction enzymes were obtained from MBI-Fermentas (St. Leon-Roth, Germany) and New England Biolabs (Frankfurt, Germany). *Escherichia coli* strain XL1Blue (Stratagene, Heidelberg) was used for amplification of plasmids. All cloning was performed using standard procedures. The expression vectors for the production of the individual myosin constructs were based on the extrachromosomal vector pDXA-3H (14). Two types of N-terminally modified *Dictyostelium* myosin-2 constructs were generated:  $\Delta$ N1-constructs have the first N-terminal 80 amino acids deleted and  $\Delta$ N2-constructs have residues Y34-N78, corresponding to the SH3-like domain, replaced with the tripeptide GTG (Figure 1).

Plasmid pSA1 encodes for the expression of full-length *Dictyostelium* myosin-2 and carries the sequence of a C-terminal His<sub>8</sub>-tag as described previously (15). PCR-directed mutagenesis using pSA1 as template resulted in the generation of myosin constructs p $\Delta$ N1-myosin and p $\Delta$ N2-myosin encoding full-length myosin-2 with completely or partially truncated N-terminus, respectively. In p $\Delta$ N2-myosin the base triplets encoding Tyr34 to Asn78 were deleted and replaced with the sequence GGTACCGGT to introduce a *Kpn*I-AgeI site in the pSA1 plasmid. The N-terminal sequence was changed to introduce a *Bam*HI site. Accordingly, the N-terminus of  $\Delta$ N2-myosin starts with Met-Asp-Pro and residues Tyr34 to Asn78 are replaced by the tripeptide Gly-Thr-Gly (Fig.1). Subcloning of the 2-kb *Sall*-*Bst*XI gene fragments from p $\Delta$ N1-myosin or p $\Delta$ N2-myosin into pM761 (16) produced constructs p $\Delta$ N1-M761 and p $\Delta$ N2-M761, respectively, encoding the myosin-2 motor domain with truncated N-terminus. *Dictyostelium* AX3-ORF<sup>+</sup> cells were used for the production of the motor domain constructs. Wild-type myosin and N-terminal truncated full-length myosins  $\Delta$ N1-myosin and  $\Delta$ N2-myosin were produced in the mhcA<sup>-</sup> null cell line HS1 (17). Transformations were performed by electroporation (18). Transformants were screened for protein production as described previously (15). Cell lines producing near wild-type levels of the recombinant myosins were selected for further analysis.

**Protein expression and purification** – *Dictyostelium* AX3-ORF<sup>+</sup> cells producing the motor domain constructs and  $\Delta$ N2-myosin myosins were grown as described previously (15). Cells producing  $\Delta$ N1-myosin myosin were grown on 26cm x 26cm plastic plates filled with 100mL HL-5C medium. The confluent plates were incubated additionally for 24 hours on gyratory shakers at 40 rpm before harvesting. Myosin null cells (HS1) transformed with pSA1, p $\Delta$ N1-myosin or p $\Delta$ N2-myosin

produced levels of full-length myosin and N-terminally truncated myosins similar to that of wild-type AX3-ORF<sup>+</sup>-cells (data not shown). The differences in molecular weight between the myosins were determined by SDS-PAGE using a 4 to 12% gradient (data not shown). The motor domain constructs were purified by Ni<sup>2+</sup>-NTA chromatography giving yields of 4 mg per g of cells for M761, 0.5 mg per g of cells for  $\Delta$ N1-M761 and 1mg per g of cells for  $\Delta$ N2-M761. Some minor modifications were made for the purification of  $\Delta$ N1-M761. Because of its lower thermal stability and increased propensity to aggregate,  $\Delta$ N1-M761 was purified in the presence of 100 mM KCl and centrifugation was performed at 30,000 g. All buffers contained 100mM KCl and centrifugation steps were changed from 230,000 g for 1 hour to 25,000 g for 30min and from 500,000 g for 1 hour to 75,000 g for 30min. Purified  $\Delta$ N1-M761 was concentrated by dialysis against solid sucrose. The ATPase activity of  $\Delta$ N1-M761 was greatly reduced after frozen storage of the protein. Therefore, we determined the time dependent reduction of the protein's actin-activated ATPase activity upon storage on ice. This showed that  $\Delta$ N1-M761 displayed no significant reduction in enzymatic activity during the first 48 hours. The results shown here were obtained with  $\Delta$ N1-M761 from five different preparations and all measurements were performed within 24 hours after elution of the protein from the Ni<sup>2+</sup>-NTA column. The results shown for  $\Delta$ N2-M761 and the myosin constructs with a complete tail region are based on at least three separate preparations.

Following purification by Ni<sup>2+</sup>-NTA affinity chromatography (15), yields of 0.5, 1.5, and 4.0 mg of purified protein were obtained for  $\Delta$ N1-M761,  $\Delta$ N2-M761 and M761 per gram of cells. The reduced yields that were obtained with  $\Delta$ N1-M761 and  $\Delta$ N2-M761 result from increased losses during the initial steps of the purification including the wash step prior to ATP-extraction of the recombinant motor domains.

Full-length myosins were prepared by the method of Ruppel *et al.* (19) with some modifications: after lysis, centrifugation and washing, the myosins were extracted from pellets with extraction buffer containing 10mM HEPES pH7.4, 125mM NaCl, 3mM MgCl<sub>2</sub>, 1mM DTT, and 3 mM ATP. After dialyses against the buffer containing 10mM PIPES pH 6.8, 50mM NaCl, 10mM MgCl<sub>2</sub> and 1mM DTT, the precipitated myosins were resolved in extraction buffer containing 300mM NaCl. The assembly-disassembly cycle was repeated again with 10-fold of the PIPES buffer without NaCl and myosins were resolved in 0.2 vol/g cell of storage buffer containing 10mM HEPES pH7.4, 250mM NaCl, 1mM DTT, 3mM MgCl<sub>2</sub> and 2 mM ATP. The purified myosins were treated with *Dictyostelium* myosin light chain kinase as described by Ruppel *et al.* Rabbit actin was purified and labeled with pyrene (pyrene-actin) as

previously described (20). The concentrations of the recombinant *Dictyostelium* myosin motor domains were determined by Bradford assay.

**Direct functional assays** – Actin-sliding motility was performed at 30°C using a fluorescence microscope as described previously (21) with some minor modifications. Assay buffer (AB) contained 10mM DTT. Experimental flow cells were constructed using BSA (0.5 mg/mL in buffer AB) coated glass slides and nitrocellulose coated coverslips. Myosins were actin-affinity purified immediately before to use, in order to remove rigor-forming myosins, as described by Uyeda *et al.* (22). The sliding movement started by introducing of 2mM ATP in BSA/anti-fade solution containing 0.5% methylcellulose.

**Kinetic measurements** – Stopped-flow measurements were performed at 20°C with a Hi-tech Scientific SF61 or an Applied Photophysics PiStar stopped-flow spectrophotometer using procedures and kinetic models described previously (23-25). All concentrations refer to the concentration of the reactants after mixing in the stopped-flow observation cell. A notation is used that distinguishes between rate and equilibrium constants in the presence and absence of actin by using bold ( $\mathbf{k}_{+1}$ ,  $\mathbf{K}_1$ ) versus italics type ( $k_{+1}$ ,  $K_1$ ); subscript A and D refer to actin ( $\mathbf{K}_A$ ) and ADP ( $\mathbf{K}_D$ ), respectively. Steady state ATPase activities were determined at 25°C using a linked enzyme assay and analyzed as describe (26). The myosin concentration was 0.5 to 1 $\mu$ M and the highest actin concentration 60 $\mu$ M. NADH oxidation was followed using the change in absorption at 340 nm in Beckmann DU-650 spectrophotometer (Beckmann, Dreeich, Germany). Conditions: 25 mM imidazole, 25 mM KCl, 4 mM MgCl<sub>2</sub>, 0.5 mM DTT, 0.5 mM ATP, 0.2 mM NADH, 0.5 mM PEP, 0.02 mg/mL LDH, 0.05 mg/mL PK, pH 7.4. The error bars shown in the graphs represent the standard deviations from at least 15 determinations of each data point. Protein from 3 or more preparations per construct was used for the generation of the graphs.

## RESULTS

### *Kinetic properties of $\Delta$ N1-M761 and $\Delta$ N2-M761 –*

To analyze in detail the effects of the truncations on the interaction with nucleotides and F-actin, steady-state ATPase measurements and transient kinetics measurements were performed. For each construct the actin-activated ATPase activity was measured over the range from 0 to 80  $\mu$ M F-actin. In the presence of saturating concentrations of ATP and in the absence of F-actin, the basal ATPase activity of  $\Delta$ N1-M761 was 0.014 s<sup>-1</sup> and thus approximately 2-fold slower than the value determined for M761. The basal ATPase rate of  $\Delta$ N2-M761 was 0.05 s<sup>-1</sup> (Table I). At concentrations of actin much lower than  $K_{app}$ , the dependence of the ATPase rate on the concentration of F-actin could be fitted to a straight line. The apparent second order rate constant for F-actin binding  $K_{app}/k_{cat}$  of the reaction could be

determined from the slope of this line. A more than 30-fold reduction in  $K_{app}/k_{cat}$  was observed for  $\Delta$ N1-M761 compared to a less than 2-fold reduction for  $\Delta$ N2-M761 (Table I). At saturating actin concentrations,  $k_{cat}$  values of 0.4 s<sup>-1</sup> and 0.9 s<sup>-1</sup> were determined for  $\Delta$ N1-M761 and  $\Delta$ N2-M761. The corresponding value for M761 is 2.1 s<sup>-1</sup>.

Binding of ATP to myosin motor domains in the absence of actin was monitored by the increase of intrinsic protein fluorescence following the addition of excess ATP and analyzed according to the model shown in Scheme 1, where the asterisks indicate changes in intrinsic protein fluorescence. The amplitude of the fluorescence signal obtained with M761 and  $\Delta$ N2-M761 was 17% and showed little change in the range from 50  $\mu$ M to 2 mM ATP. In the case of  $\Delta$ N1-M761, addition of less than 250  $\mu$ M ATP produced a more than 5-fold smaller change in intrinsic protein fluorescence and at higher ATP concentrations the signal change became too small to allow accurate rate determinations. The observed rate constants ( $k_{obs}$ ) for the exponential increase in protein fluorescence were linearly dependent on the concentration of ATP up to 100  $\mu$ M. The apparent second order rate constant for ATP binding to myosin ( $K_1k_{+2}$ ) is defined by the slope of the best-fit line and could be determined for all three constructs. Values of  $K_1k_{+2}$  for ATP binding were similar for wild-type myosin M761 and  $\Delta$ N2-M761 and 3-fold faster for  $\Delta$ N1-M761 (Table II). At high ATP concentrations (> 2 mM) the observed rate constants for M761 and  $\Delta$ N2-M761 saturate, and the dependence on the ATP concentration could be described by a hyperbola, where the maximum value of  $k_{obs}$  defines  $k_{+2}$ , the rate of the conformational change that follows ATP binding and precedes ATP-hydrolysis (Scheme 1).

The change observed upon the addition of ADP was too small to measure for all three constructs. Therefore, additional measurements were performed using the fluorescent analogues mantATP and mantADP to measure nucleotide binding (27). Binding of mant-nucleotides was determined by monitoring the increase in mant-fluorescence upon the addition of increasing concentrations of the fluorescent nucleotides to the motor domain constructs. In the range from 1 to 25  $\mu$ M, the observed rate constants ( $k_{obs}$ ) for the exponential increase in fluorescence were linearly dependent on the concentration of mant-nucleotide. The apparent second order rate constants were determined from the slope of the plotted best-fit line (data not shown). The rate for mantATP binding was similar for all constructs. Similarly, the second order rate constants for mantADP binding ( $k_{+D}$ ) displayed less than 3-fold differences (Table II). The rate of mantADP dissociation ( $k_{-D}$ ) was determined by monitoring the decrease in fluorescence upon displacement of mantADP from the myosin•mantADP complex by the addition of excess ATP. The observed process could be fitted to a single exponential (Figure 2) with  $k_{obs}$  corresponding directly to the dissociation

rate  $k_{-D}$  (see Scheme 1). Compared to M761 and  $\Delta N2$ -M761 the rate of mantADP release from  $\Delta N1$ -M761 was more than 30-fold decreased (Figure 2, insert). Therefore, the almost 100-fold increase in ADP-affinity displayed by  $\Delta N1$ -M761 is mostly caused by the slower rate of ADP-dissociation.

The rate of F-actin binding was measured by following the exponential decrease in pyrene fluorescence observed upon binding of excess pyrene-labeled F-actin to myosin head fragments (16). The change in pyrene fluorescence could be fitted to a single exponential function. The observed rate constants were linearly dependent upon F-actin concentration over the entire range studied (Figure 3A). The apparent second-order rate constants for pyr-actin binding ( $k_{+A}$ ) were obtained from the slopes of the plotted line. Values of  $1.2 \times 10^6 \text{ M}^{-1}\text{s}^{-1}$  for M761,  $0.19 \times 10^6 \text{ M}^{-1}\text{s}^{-1}$  for  $\Delta N1$ -M761, and  $0.10 \times 10^6 \text{ M}^{-1}\text{s}^{-1}$  for  $\Delta N2$ -M761 were obtained. The rate of F-actin dissociation ( $k_{-A}$ ) from the myosin constructs was determined from the rate of fluorescence enhancement observed by displacing pyr-actin from pyr-acto•M with an excess of unlabeled actin (Figure 3B). M761 and  $\Delta N2$ -M761 displayed smaller than 2-fold differences in the rate of actin displacement. In contrast, F-actin dissociation from  $\Delta N1$ -M761 was 9-fold increased (Figure 3 B, insert). The dissociation equilibrium constants for actin binding ( $K_A$ ) defined by the ratio  $k_{-A}/k_{+A}$  shows that the actin affinities for  $\Delta N1$ -M761 and  $\Delta N2$ -M761 are ~100-times and ~20-times lower than the value obtained for M761 (Table III). These differences explain at least in part the differences in the yields obtained for the different constructs during purification.

Addition of excess ATP to pyr-actomyosin complexes results in an exponential increase in pyrene fluorescence as the actin dissociates. Values of  $k_{obs}$  were linearly dependent on ATP concentration in the range from 5- 25  $\mu\text{M}$  (data not shown). The slope of the best-fit line defines the apparent second-order rate constant  $K_1 k_{+2}$ , values of  $2.3 \times 10^5 \text{ M}^{-1}\text{s}^{-1}$ ,  $5.9 \times 10^5 \text{ M}^{-1}\text{s}^{-1}$ , and  $1.7 \times 10^5 \text{ M}^{-1}\text{s}^{-1}$  were obtained for M761,  $\Delta N1$ -M761, and  $\Delta N2$ -M761 (Table III)

The affinity of ADP for pyr-acto•M was determined from the ADP inhibition of the ATP-induced dissociation of actin from the complex. Mixing of 0.25M pyr-acto•M with 100  $\mu\text{M}$  ATP in the presence of different amounts of ADP results in an exponential increase in intrinsic protein fluorescence. No signal was obtained with  $\Delta N1$ -M761. An increase in the concentration of ADP produced a reduction in  $k_{obs}$  for  $\Delta N2$ -M761 and M761 constructs. The estimated  $K_{AD}$  values, obtained from fitting the data to equation 2 were 15  $\mu\text{M}$  for  $\Delta N2$ -M761 and 182  $\mu\text{M}$  for M761 (Table III).

**Functional analysis** – The motor activity of the purified myosins was analyzed using *in vitro* motility assays (28,29).  $\Delta N1$ -myosin and  $\Delta N2$ -

myosin supported the movement of actin filaments with velocities of 48 nm/sec and 340 nm/sec, respectively. In comparison, actin filaments moved with a velocity of 2.6  $\mu\text{m}/\text{sec}$  on surfaces decorated with wild-type myosin (Fig. 4).

Complementation assays with myosin-2 null-cells were used to test the constructs ability to rescue myosin-2-dependent processes.  $\Delta N1$ -myosin and  $\Delta N2$ -myosin were produced at a level similar to that of endogenous myosin-2 in wild-type cells. *Dictyostelium* myosin-2 null-cells display characteristic phenotypic alterations that affect cytokinesis and the multicellular stages of *Dictyostelium* development. Complementation of myosin null-cells with  $\Delta N1$ -myosin did not rescue any of the myosin-2 specific defects. Transformants were unable to undergo normal cytokinesis, they were unable to grow in suspension culture, and their development was blocked at the mound stage (Fig. 5). In contrast, myosin-2 null-cells transformed with  $\Delta N2$ -myosin constructs were phenotypically almost normal. They grew at the same rate as null-cells that were transformed with a myosin-2 wild-type construct and they produced viable spores, although their fruiting bodies were markedly smaller than those formed by *Dictyostelium* cells producing wild-type myosin-2 (Fig. 5).

## DISCUSSION

The N-terminal subdomain of myosin-2 is one of the least conserved regions within the myosin head. Although class-1 myosins completely lack this region, it is clear from our *in vivo* functional analysis that the region or part of it is important for the normal functioning of a class-2 myosin. The kinetic analysis of  $\Delta N1$  and  $\Delta N2$ -myosin constructs reveals that the N-terminal truncations affect but do not abolish the ability of myosin to bind nucleotides, to hydrolyze ATP or to interact with F-actin. The truncations neither change the apparent affinity for ATP in the absence of actin nor do they greatly perturb the basal  $\text{Mg}^{2+}$ -ATPase rate. Actin-activation of ATPase activity is also maintained in these constructs.

The transient-kinetic characterization of  $\Delta N1$ -M761 that lacks the complete N-terminal subdomain proved to be difficult, due to the weakness or complete absence of spectroscopic signals associated with the binding of nucleotides.  $\Delta N1$ -M761 binds at least 80-fold more weakly to F-actin and dissociates 12-times faster from F-actin in the absence of nucleotides. The weak interaction with F-actin, which is also apparent in the presence of nucleotides, correlates well with a reduced activation of ATPase activity and a reduction in the maximum turnover rate  $k_{cat}$ . In addition, the 40-fold decrease in the rate of mantADP release indicates that ADP-release may become the rate-limiting step for basal ATPase, which is also apparent from the close similarity of the rate constants  $k_{-D}$  and  $k_{basal}$  measured for  $\Delta N1$ -M761.

Head domain construct  $\Delta$ N2-M761 shows almost wild-type like kinetic properties with binding and release rates for mantADP similar to M761. The observed 6-fold and 8-fold reductions in catalytic ( $k_{\text{cat}}$ ) and motor activities ( $V_{\text{max}}$ ) of  $\Delta$ N2-myosin can be linked to perturbations in F-actin binding, ADP binding, and coupling between the actin and nucleotide binding sites. These perturbations include an 18-fold decreased F-actin affinity in the absence of nucleotides ( $K_A$ ), a 12-fold increased affinity for ADP in the actin-bound state ( $K_{AD}$ ), and an almost 7-fold reduced coupling ratio ( $K_{AD}/K_D$ ).

$\Delta$ N1-myosin and  $\Delta$ N2-myosin support actin-filament movement. The 54-fold and 8-fold reduced velocities correlate well with the observed changes in the rates of ADP release that were observed for  $\Delta$ N1-myosin and  $\Delta$ N2-myosin, respectively. In the presence of a saturating number of myosin motors, velocity is proportional to  $d/t_s$ , where  $d$  is the stroke size, and  $t_s$  is the strongly bound state time. The  $t_s$  is independent of total ATP hydrolysis time and is determined by the rate of ADP release. The reduced velocities can therefore be directly attributed to a slow ADP release rate and a high ADP affinity for acto-myosin (23).

The results of *in vitro* motility assays with  $\Delta$ N1-myosin and  $\Delta$ N2-myosin explain at least in part the phenotypic changes observed for myosin null-cells producing the truncated myosins.  $\Delta$ N1-myosin displays a more than 50-fold reduced motility in the assay and is not able to compensate the myosin-dependent defects, when produced in null-cells. In contrast,  $\Delta$ N2-myosin displays an only 7-fold reduced motile activity and complementation assays with  $\Delta$ N2-myosin indicate almost normal myosin-2 function. This observation suggests that the SH3-like subdomain is not critical for the *in vivo* function of myosin-2 under the conditions examined.

Several earlier studies have addressed the interactions of the N-terminal region with other regions of the myosin head fragment. Using changes in intrinsic protein fluorescence, Berger and colleagues concluded that the SH3-like subdomain of smooth muscle myosin is conformationally sensitive to nucleotide binding and/or hydrolysis. They further suggested that the N-terminal region is only indirectly coupled to the active site but that it is sensitive to direct interactions with the lever arm in the strongly bound states of the ATPase cycle (30,31). Contacts between the N-terminus and heavy chain residues 750–760 in the converter region (*Dictyostelium discoideum* numbering) have been implicated by differential scanning calorimetry (DSC) as important for the structural integrity and stability of the entire motor domain (32). Following tryptic cleavage of the skeletal muscle myosin heavy chain between Arg-23 and Ile-24, Levitsky and coworkers observed a reduction of the thermal transition from 49° C to 42° C, while nucleotide binding was unaffected (32). In contrast, tryptic cleavage in loop 1 and loop 2 did neither affect the thermal transition temperature nor nucleotide

binding. In agreement with these observations, we found that the  $\Delta$ N1-constructs displayed an almost complete loss of enzymatic activity within 48 hours after their purification.  $\Delta$ N1-M761 displayed complete loss of activity following freeze thawing. The importance of contacts between N-terminal residues and residues 750–760 in the converter is supported by similarities in the kinetic behavior of  $\Delta$ N1-M761 and M754, a motor domain construct that is truncated at position 754 of the myosin heavy chain.

In conclusion, our experiments show that the initial 33 N-terminal residues are of great importance for normal communication between the functional regions within the myosin-2 motor domain. Based on the observed differences between the crystal structures of class-1 and class-2 motor domains (33-35), we suggest that the N-terminal residues Pro3, Ile4, Tyr11, Leu15, and Tyr14 play an important role because they stabilize the motor domain through clustered hydrophobic interactions with residues Pro133, Ile134, Met139, Ile142, Phe143, and His154 in the proximal part of the N-terminal region (Fig. 1 b, c). Additional structural stability in this region is maintained by hydrophobic interactions formed between residues Phe25-to-Lys32 and residues 760-to-765 on an adjacent helix that emerges from the converter region (Fig. 1 a). Hence, non-covalent attractive forces between the N-terminal and C-terminal region of the motor domain are important for the structural and functional integrity of the myosin motor. Removal of only the SH3-like subdomain, as performed in the  $\Delta$ N-2-constructs, does not affect the biological function of myosin-2 in *Dictyostelium*. However, the replacement of the SH3-like subdomain has still a clear effect on the way in which conformational changes that follow the binding of F-actin or nucleotide are communicated within the motor domain. At this stage, it is tempting to speculate that the mechanical perturbations of the SH3-like subdomain, as they may occur in the sarcomere, the crowded context of a cleavage furrow or in other physiological situations, can lead to changes in the functional behavior of the motor that are in their extent similar or even greater than those observed for  $\Delta$ N-2-myosin. The way in which intra- and intermolecular contacts (30), modifications and substitutions of light chains (36) may affect or modulate the communication pathway via the SH3-like subdomain and whether such a pathway is important for the regulation and functional fine-tuning of at least some myosins remains to be elucidated in further studies.

*Acknowledgements* – We thank R. Schumann and S. Zimmermann for excellent technical assistance, R. Fedorov for providing figure 1, and M.A. Geeves, N. Tzvetkov and R. Fedorov for discussions. The work was supported by grant MA1081/5-3 from the Deutsche Forschungsgemeinschaft.

## REFERENCES

1. Sellers, J. R. (2000) *Biochim. Biophys. Acta* **1496**, 3-22
2. Holmes, K. C., Schröder, R. R., Sweeney, H. L., and Houdusse, A. (2004) *Philos. Trans. R. Soc. Lond. B. Biol. Sci.* **359** (1452), 1819-1828
3. Geeves, M. A., Fedorov, R., and Manstein, D. J. (2005) *Cell Mol Life Sci.* **62**, 1462-1477
4. Menetrey, J., Bahloul, A., Wells, A. L., Yengo, C. M., Morris, C. A., Sweeney, H. L., and Houdusse, A. (2005) *Nature* **435**, 779-785
5. Coureux, P. D., Wells, A. L., Menetrey, J., Yengo, C. M., Morris, C. A., Sweeney, H. L., and Houdusse, A. (2003) *Nature* **425**, 419-423
6. Smith, C. A., and Rayment, I. (1996) *Biochemistry* **35**, 5404-5417
7. Schroder, R. R., Manstein, D. J., Jahn, W., Holden, H., Rayment, I., Holmes, K. C., and Spudich, J. A. (1993) *Nature* **364**, 171-174
8. Dominguez, R., Freyzon, Y., Trybus, K. M., and Cohen, C. (1998) *Cell* **94**(5), 559-571
9. Kollmar, M., Durrwang, U., Kliche, W., Manstein, D. J., and Kull, F. J. (2002) *EMBO J.* **21**, 2517-2525
10. Koch, C. A., Anderson, D., Moran, M. F., Ellis, C., and Pawson, T. (1991) *Science* **252**, 668-674
11. Onishi, H., Maita, T., Matsuda, G., and Fujiwara, K. (1990) *J. Biol. Chem.* **265**, 19362-19368
12. Ito, K., Liu, X., Katayama, E., and Uyeda, T. Q. (1999) *Biophys. J.* **76**, 985-992
13. Schröder, R. R., Manstein, D. J., Jahn, W., Holden, H., Rayment, I., Holmes, K. C., and Spudich, J. A. (1993) *Nature* **364**, 171-174
14. Manstein, D. J., Schuster, H. P., Morandini, P., and Hunt, D. M. (1995) *Gene* **162**, 129-134
15. Manstein, D. J., and Hunt, D. M. (1995) *J. Muscle Res. Cell Motil.* **16**, 325-332
16. Kurzawa, S. E., Manstein, D. J., and Geeves, M. A. (1997) *Biochemistry* **36**, 317-323
17. Manstein, D. J., Titus, M. A., De Lozanne, A., and Spudich, J. A. (1989) *EMBO J.* **8**, 923-932
18. Egelhoff, T. T., Titus, M. A., Manstein, D. J., Ruppel, K. M., and Spudich, J. A. (1991) *Meth. Enzymol.* **196**, 319-334
19. Ruppel, K. M., Uyeda, T. Q., and Spudich, J. A. (1994) *J. Biol. Chem.* **269**, 18773-18780
20. Criddle, A. H., Geeves, M. A., and Jeffries, T. (1985) *Biochem. J.* **232**(2), 343-349
21. Anson, M., Geeves, M. A., Kurzawa, S. E., and Manstein, D. J. (1996) *EMBO J.* **15**, 6069-6074
22. Uyeda, T. Q., Kron, S. J., and Spudich, J. A. (1990) *J. Mol. Biol.* **214**, 699-710
23. Batra, R., Geeves, M. A., and Manstein, D. J. (1999) *Biochemistry* **38**(19), 6126-6134
24. Furch, M., Fujita-Becker, S., Geeves, M. A., Holmes, K. C., and Manstein, D. J. (1999) *J. Mol. Biol.* **290**, 797-809
25. Tsiavaliaris, G., Fujita-Becker, S., Batra, R., Levitsky, D. I., Kull, F. J., Geeves, M. A., and Manstein, D. J. (2002) *EMBO Rep.* **3**, 1099-1105
26. Furch, M., Geeves, M. A., and Manstein, D. J. (1998) *Biochemistry* **37**, 6317-6326
27. Woodward, S. K., Geeves, M. A., and Manstein, D. J. (1995) *Biochemistry* **34**, 16056-16064
28. Kron, S. J., and Spudich, J. A. (1986) *Proc. Natl. Acad. Sci. U.S.A.* **83**, 6272-6276
29. Kron, S. J., Toyoshima, Y. Y., Uyeda, T. Q., and Spudich, J. A. (1991) *Methods Enzymol.* **196**, 399-416
30. van Duffelen, M., Chrin, L. R., and Berger, C. L. (2005) *Biochem Biophys. Res Commun.* **329**, 563-572
31. van Duffelen, M., Chrin, L. R., and Berger, C. L. (2004) *Biophys. J.* **87**, 1767-1775
32. Nikolaeva, O. P., Orlov, V. N., Bobkov, A. A., and Levitsky, D. I. (2002) *Eur. J. Biochem.* **269**, 5678-5688
33. Fisher, A. J., Smith, C. A., Thoden, J. B., Smith, R., Sutoh, K., Holden, H. M., and Rayment, I. (1995) *Biochemistry* **34**, 8960-8972
34. Reubold, T. F., Eschenburg, S., Becker, A., Kull, F. J., and Manstein, D. J. (2003) *Nat. Struct. Biol.* **10**, 826-830
35. Kollmar, M., Dürrwang, U., Kliche, W., Manstein, D. J., and Kull, F. J. (2002) *EMBO J.* **21**(11), 2517-2525
36. Terrak, M., Rebowski, G., Lu, R. C., Grabarek, Z., and Dominguez, R. (2005) *Proc. Natl. Acad. Sci. U.S.A.* **102**(36), 12718-12723

## FOOTNOTES

<sup>1</sup> The abbreviations used are: ELC, myosin-2 essential light chain; M761, *D. discoideum* myosin-2 motor domain; ΔN1-M761, *D. discoideum* myosin-2 motor domain lacking the 80 N-terminal residues; ΔN2-constructs have residues Y34-N78 replaced with the tripeptide GTG; F-actin, filamentous actin; HEPES, N-(2-hydroxyethyl)-piperazine-N'-2-ethanesulfonic acid; N.D., not determined; TRITC, tetramethyl rhodamine isothiocyanate.

## FIGURE LEGENDS

**FIGURE 1. Structure of the myosin-2 motor domain and its N-terminal region.** *A*, Ribbon representation of the *Dictyostelium* myosin-2 motor domain (34). Residues 81-689 of the motor domain are shown in green. The N-terminal region corresponding to residues 2-33 is shown in yellow. The SH3-like subdomain formed by residues 34-78 (yellow) was truncated in constructs  $\Delta$ N2-M761 and  $\Delta$ N2-myosin. The entire N-terminal region formed by residues 2-80 was truncated in constructs  $\Delta$ N1-M761 and the equivalent full-length construct  $\Delta$ N1-myosin. The converter region and the C-terminal  $\alpha$ -helix emerging from the motor domain (residues 690-770) are shown in blue. Hydrophobic interactions formed between residues 760-to-765 in this helix and residues Phe25-to-Lys32 provide additional structural stability. *B*, Hydrophobic interactions formed between the N-terminal region and the core motor domain. Ribbon representation and electrostatic surface potential of the 80 amino acid long N-terminal region of *Dictyostelium* myosin-2. Negatively charged residues are labeled in red, non-charged residues are colored in white and positively charged residues in blue. Hydrophobic side chains Pro3, Ile4, Tyr11, Leu15 and Tyr14 (yellow), shown as ball-and-stick model, are part of a disordered loop (red) facing a groove formed by hydrophobic residues Pro133, Ile134, Met139, Ile142, Phe143 and His154 (white surfaces). *C*, The view from (B) rotated by 90°. *D*, Amino acid sequence of the *Dictyostelium* myosin-2 N-terminus. The N-terminal region of wild-type myosin-2 comprises the first 80 amino acids. This region has been removed in  $\Delta$ N1-myosin and the corresponding motor domain construct  $\Delta$ N1-M761. In the  $\Delta$ N2-constructs only the SH3-like domain (residues Tyr34 to Asn78) has been replaced by the tripeptide Gly-Thr-Gly. The Figure was prepared using the programs WebLab Viewer Lite 4.0 (Molecular Simulations Inc. 2000) and POV-Ray 3.6 (Persistence of Vision Ray Tracer v3.02, 1997, <http://www.povray.org>).

**FIGURE 2. Rate of mantADP displacement from myosin head fragments.** Stopped-flow records of fluorescence decrease upon binding of 200  $\mu$ M ATP to 0.5  $\mu$ M myosin construct, premixed with 0.5  $\mu$ M mantADP. M761 and  $\Delta$ N2-M761 show similar rates of mantADP-displacement of 1.6 and 1.3  $s^{-1}$ , respectively. MantADP release from  $\Delta$ N-1 is approximately 40-times slower (insert). The observed dissociation rate constants ( $k_D$ ) are summarized in Table II.

**FIGURE 3. Interaction of pyrene-actin with myosin head fragments.** *A*, Dependence of the rate of pyrene-actin binding to myosin head fragments on pyrene-actin concentration. The data were fit to a straight line, the slope of which gives the second-order rate constants for binding to actin ( $k_{+A}$ ). All of the resulting values are summarized in Table III. (■) M761, (○)  $\Delta$ N1-M761, (□)  $\Delta$ N2-M761. *B*, The dissociation rate constants ( $k_A$ ) for each myosin construct was determined from the rate of fluorescence enhancement that followed the addition of excess unlabeled actin to pyrene-actin equilibrated myosin head fragment. The solid line is the best fit to single exponential function giving values for ( $k_A$ ).  $\Delta$ N1-M761 displays 10-times faster actin dissociation kinetics than M761 and  $\Delta$ N2-M761. The dissociation equilibrium constant ( $K_A$ ) for actin binding was calculated from the ratios of  $k_A$  and  $k_{+A}$  (Table III). The experimental conditions were 20 mM Mops, 5 mM  $MgCl_2$ , and 100 mM KCl, pH 7.0, 20 °C.

**FIGURE 4. Sliding velocity of filamentous actin on myosin coated surfaces.** Motor function was directly analyzed by measuring the sliding velocity of rhodamine phalloidin labeled actin-filaments on myosin-coated surfaces under a fluorescence microscope (21). For each experiment, 0.25 mg/ml myosin, 20 nM rhodamine phalloidin labeled actin and 2 mM ATP were used. The movement of at least 50 filaments was followed and the average sliding velocity was determined by the analysis of the Gaussian distribution.  $\Delta$ N-1 myosin A, moved actin filaments at  $48.0 \pm 8.5$  nm/sec, *B*,  $\Delta$ N2-myosin  $342.7 \pm 43.0$  nm/sec and wild type myosin C, moved the actin-filaments at  $2.61 \pm 0.3$   $\mu$ m/sec at 30°C.

**FIGURE 5. Functional characterization of  $\Delta$ N1-myosin and  $\Delta$ N2-myosin.** *A*, Development cycle of *Dictyostelium* cells. Fruiting body formation is a myosin-2-dependent process that occurs under starvation conditions. AX3-Orf<sup>+</sup> wild type cells form fruiting bodies that consist of a long stalk and an unwalled, globose spore mass on the top. The scale bar represents 1 mm. *B*, HS1-cells in which the *mhcA* gene has been deleted are not able to undergo the complete process of fruiting body formation and sporogenesis, instead the cells stop differentiation after they have formed an aggregation mount. *C*, Complementation of myosin null-cells with the wild-type *mhcA* restores the developmental defect. *D*, Null-cells producing  $\Delta$ N1-myosin are not able to form fruiting bodies with viable spores. Their development cycle progresses only to the formation of small stem-like structures, without formation of viable spores. *E*, Complementation of myosin null-cells with  $\Delta$ N2-myosin leads to the formation of fruiting bodies with short stalks, normal spore heads, and viable spores. *F*, Cell growth in suspension culture. Individual *Dictyostelium* cell lines expressing wild-type and mutant myosins were transferred

to 100 ml HL-5C medium at densities of  $10^5$  cells per milliliter and grown on a rotary shaker at 180 rpm. (■) AX3-Orf<sup>+</sup> cells show a doubling time of ~8 hours while (○) myosin null-cells (HS1) are unable to grow in suspension. This defect is rescued by the reintroduction of the *mhcA* gene into the null-cells as shown by (□) HS1-cells expressing wild type myosin-2. (▼) HS1-cells expressing  $\Delta$ N1-myosin are not able to rescue the defect while (▲) HS1-cells producing  $\Delta$ N2-myosin grow at a similar rate as (□) HS1-cells that produce wild type myosin-2.

TABLE I

*Actin activation of ATPase activity*

The experimental conditions were 25 mM HEPES, pH 7.4; 25 mM KCl, 4 mM MgCl<sub>2</sub> at 25°C. Actin-activated ATPase activity was measured in the presence of rabbit skeletal muscle F-actin.

Myosin construct	$k_{\text{basal}}$ (s <sup>-1</sup> )	$k_{\text{cat}}$ <sup>a</sup> (s <sup>-1</sup> )	$K_{\text{app}}$ <sup>a</sup> (μM)	$k_{\text{cat}}/K_{\text{app}}$ <sup>b</sup> (μM <sup>-1</sup> s <sup>-1</sup> )
<b>ΔN1-M761</b>	0.014 ± 0.001	0.37 ± 0.15	>300	>0.001
<b>ΔN2-M761</b>	0.05 ± 0.001	0.87 ± 0.08	45 ± 2.4	0.019
<b>M761</b>	0.037 ± 0.012	2.06 ± 0.28	70.4 ± 10	0.029

<sup>a</sup> Values for  $k_{\text{cat}}$  and  $K_{\text{app}}$  were calculated from fitting the data to the Michaelis-Menten equation.

<sup>b</sup> The data at concentrations of actin much lower than  $K_{\text{app}}$ , could be fit to a straight line and the apparent second order rate constant for actin binding  $k_{\text{cat}}/K_{\text{app}}$  was determined from the slope of this line.

TABLE II

*Kinetic parameters of myosin interaction with nucleotides*

The experimental conditions were 20 mM MOPS, pH 7.0, 5 mM MgCl<sub>2</sub>, 100 mM KCl at 20°C.

Nucleotide	Rate constant	M761	ΔN1-M761	ΔN2-M761
ATP	$K_1k_{+2}$ (μM <sup>-1</sup> s <sup>-1</sup> )	0.90 ± 0.04	3.12 ± 0.10	0.60 ± 0.05
	$k_{+2}$ (s <sup>-1</sup> )	28 ± 4	N.D.	176 ± 9
mantATP	$K_1k_{+2}$ (μM <sup>-1</sup> s <sup>-1</sup> )	1.04 ± 0.02	1.03 ± 0.02	0.60 ± 0.01
mantADP	$k_{-D}$ (μM <sup>-1</sup> s <sup>-1</sup> )	0.36 ± 0.01	0.89 ± 0.01	0.45 ± 0.005
	$k_{-D}$ (s <sup>-1</sup> )	1.6 ± 0.002	0.04 ± 0.003	1.3 ± 0.002
	$K_D$ (μM)	4.45	0.045	2.9

The binding and hydrolysis of ATP by *D. discoideum* myosin head fragments was analyzed in terms of Scheme 1.  $k_{+i}$  and  $k_{-i}$  are forward and reverse rate constants and  $K_i$  ( $k_{+i}/k_{-i}$ ) is the association equilibrium constant of the *i*<sup>th</sup> step of the reaction.  $K_D$  corresponds to  $K_6K_7$ . Uncertainties represent standard errors in the best fits of the data.

TABLE III

*Kinetic parameters of myosin interaction with actin*The experimental conditions were 20 mM MOPS, pH 7.0, 5 mM MgCl<sub>2</sub>, 100 mM KCl at 20°C.

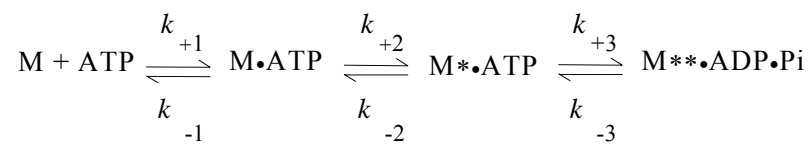
<i>Nucleotide</i>	<i>Rate constant</i>	M761	ΔN1-M761	ΔN2-M761
Nucleotide binding to actomyosin				
ATP	$K_1k_{+2}$ ( $\mu\text{M}^{-1}\text{s}^{-1}$ )	$0.23 \pm 0.01$	$0.59 \pm 0.008$	$0.17 \pm 0.02$
ADP	$K_{AD}$ ( $\mu\text{M}$ )	$210 \pm 2$	No Signal	$15 \pm 2$
	$K_{AD}/K_D$	$18 \pm 0.7$	–	$5^a$
Actin binding to myosin				
	$k_{+A}$ ( $\mu\text{M}^{-1}\text{s}^{-1}$ )	$1.22 \pm 0.1$	$0.19 \pm 0.03$	$0.10 \pm 0.01$
	$k_A$ ( $\text{s}^{-1}$ )	$0.0035 \pm 0.0005$	$0.044 \pm 0.0005$	$0.005 \pm 0.0004$
	$K_A$ (nM)	2.9	230	50
	$K_{DA}=K_A \cdot K_{AD}/K_D$ (nM)	52.2	–	250

Acto•M ATPase activity was analyzed in terms of Scheme 2. Coupling between the actin and the nucleotide binding sites was analyzed using the model shown in Scheme 3. In this scheme  $K_A$ ,  $K_{AD}$ ,  $K_{DA}$ , and  $K_D$  are defined as dissociation equilibrium constants. The presence of actin alters the affinity of ADP for myosin and vice versa. The ADP affinity for MHF is given as  $K_D$ , and the affinity of myosin for actin is defined as  $K_A$ .

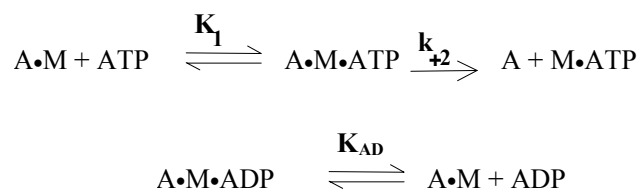
<sup>a</sup> The value for  $K_D$  was determined using mantADP instead of ADP.

Uncertainties represent standard errors in the best fits of the data.

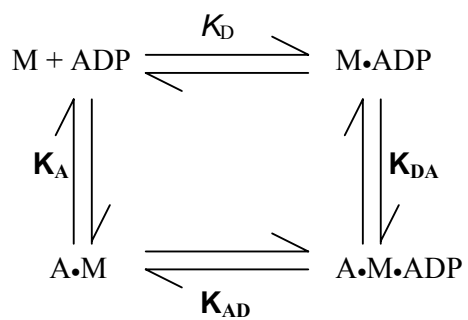
Scheme 1



Scheme 2



Scheme 3



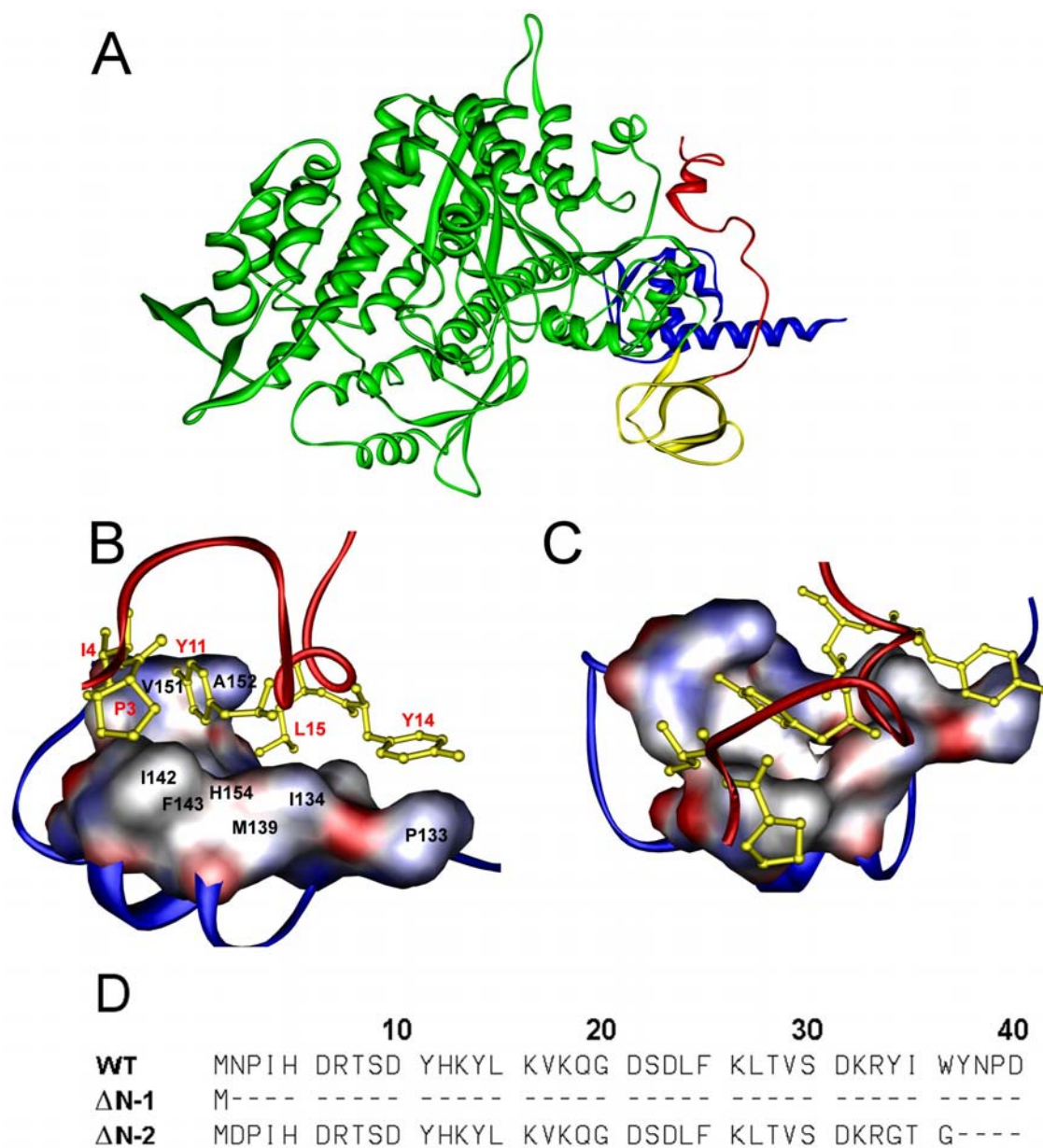


FIGURE 1

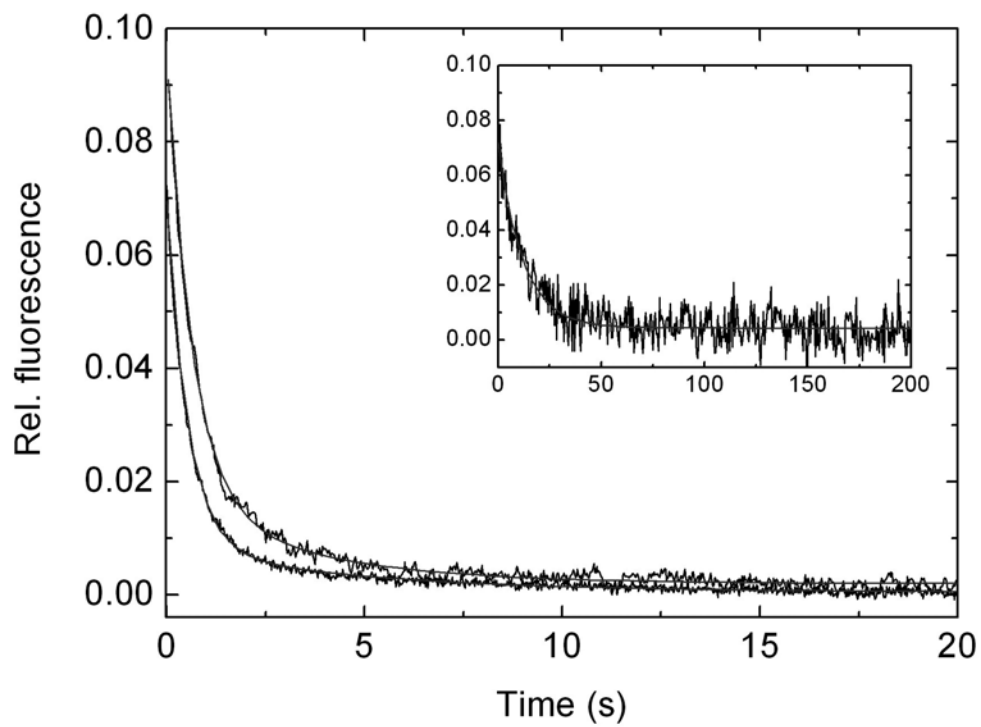


FIGURE 2

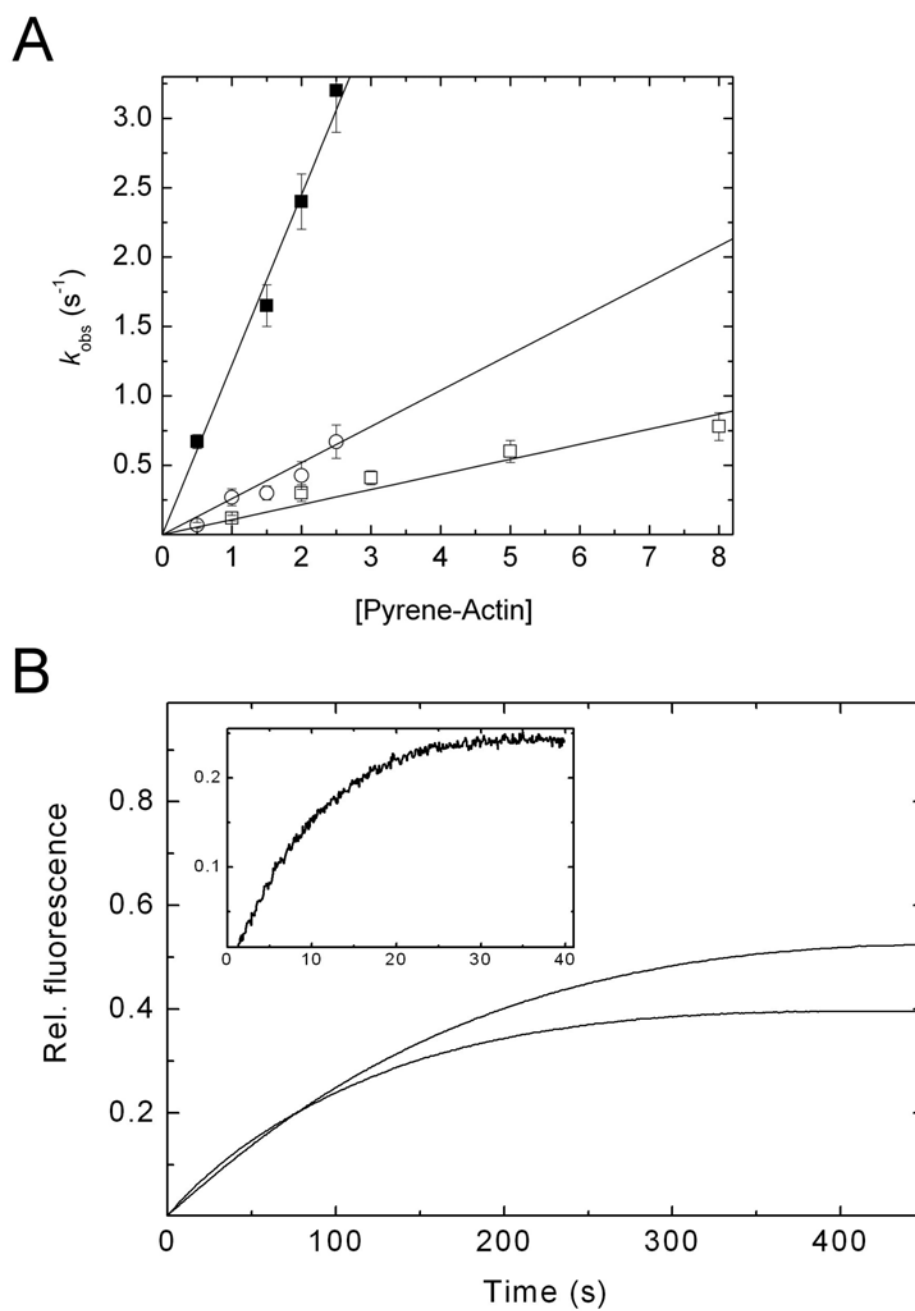


FIGURE 3

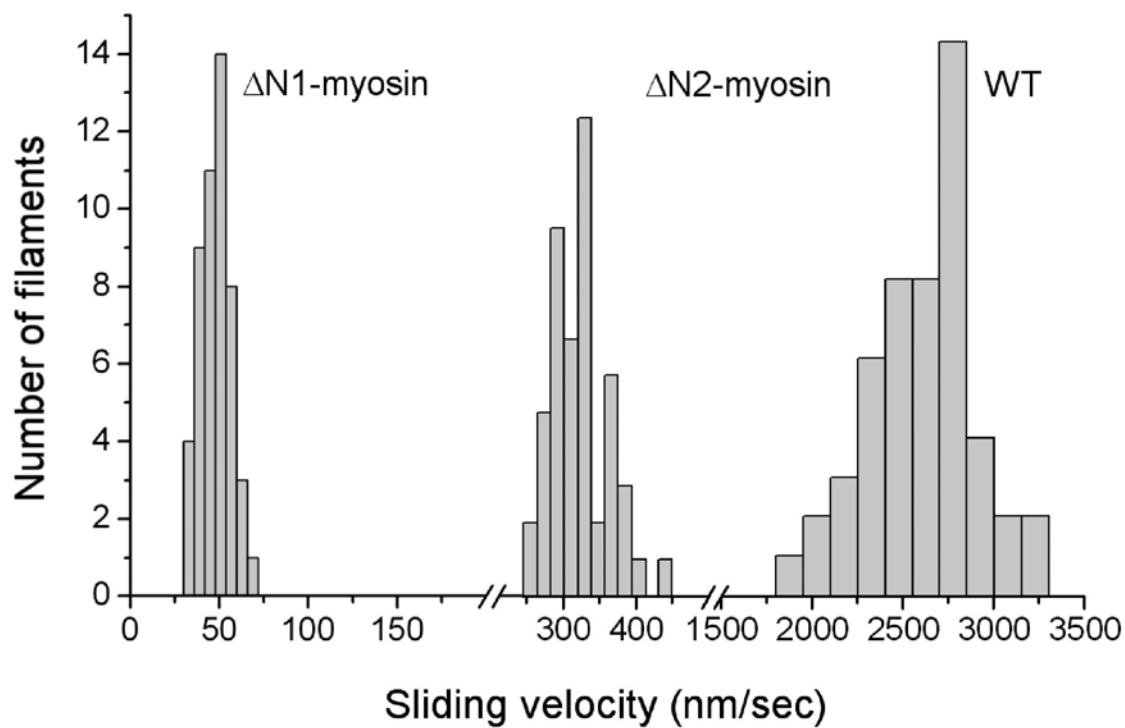


FIGURE 4

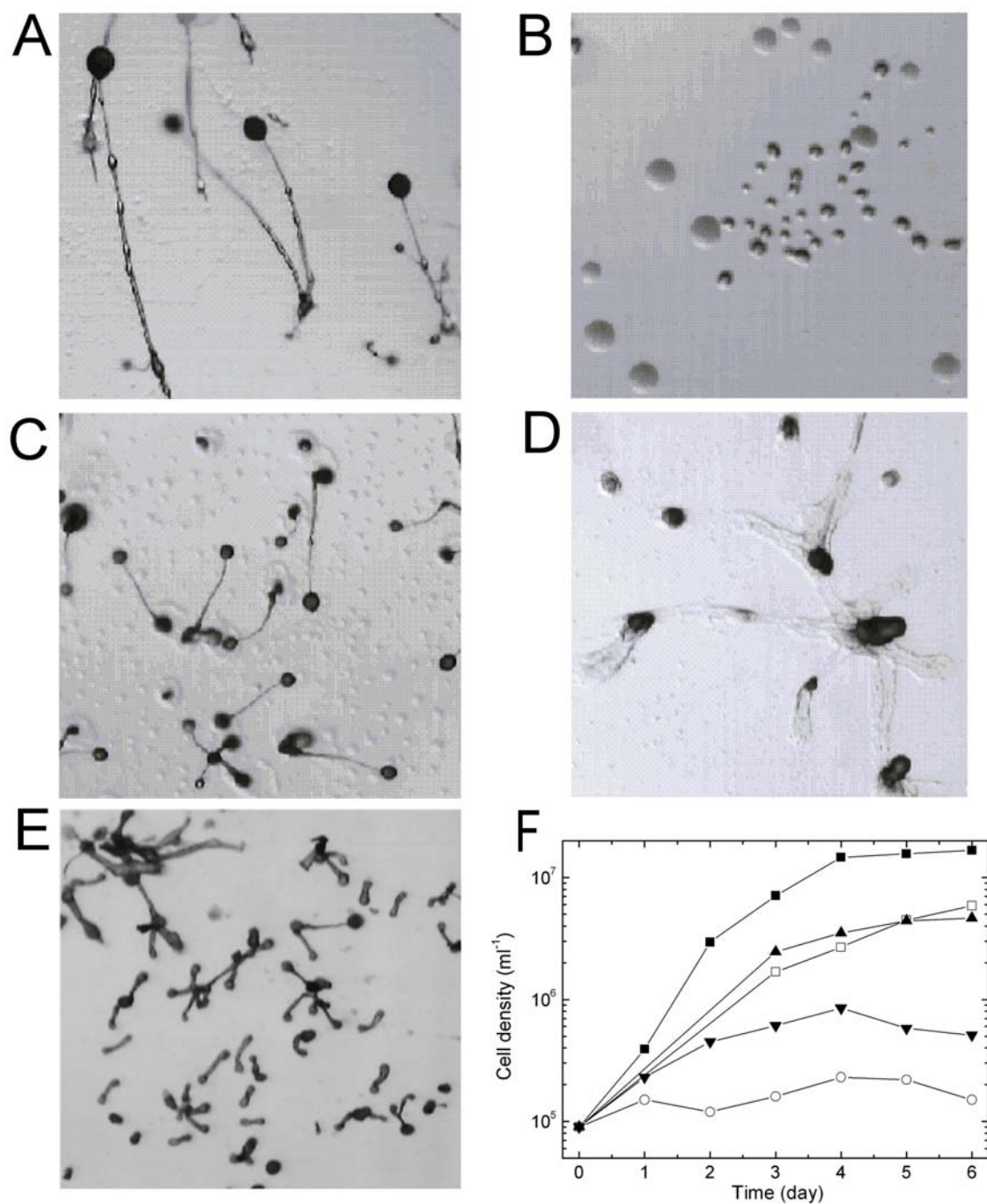


FIGURE 5